Sensitivity dependences on side length and aspect ratio of a diaphragm in a glass-based guided-wave optical pressure sensor

Hiroyuki Nikkuni,[1] Yu Watanabe,[1] Masashi Ohkawa,[2]* and Takashi Sato,[2]

[1]Graduate School of Science and Technology, Niigata University, 8050 Ikarashi 2-no-cho, Nishi-ku, Niigata 950-2181, Japan

[2] Faculty of Engineering, Niigata University, 8050 Ikarashi 2-no-cho, Nishi-ku, Niigata 950-2181, Japan

**Corresponding author: ohkawa@eng.niigata-u.ac.jp*

Abstract: According to our previous theoretical study, sensor sensitivity is proportional to the cube of the side length of the diaphragm in a guided-wave optical pressure sensor consisting of a glass diaphragm and a single-mode waveguide on the diaphragm. Also, to obtain higher sensitivity, an aspect ratio of the diaphragm should be approximately 1 for two waveguide positions: the center and the edge of the diaphragm. In this study, sensitivity dependences on side length and aspect ratio of the diaphragm were experimentally examined. The obtained experimental results strongly supported the theoretical predictions.

OCIS codes: (130.0130) Integrated optics; (130.2790) Guided-waves; (130.3120) Integrated optics devices; (130.6010) Sensors; (230.3120) Integrated optics devices; (230.7370) Waveguides.

References and links

1. M. Li, M. Wang, and H. Li, "Optical MEMS pressure sensor based on Fabry-Perot interferometry," Opt. Express **14**, 1497-1504 (2006).
2. J. Xu, X. Wang, K. L. Cooper, and A. Wang, "Miniature all-silica fiber optic pressure and acoustic sensors," Opt. Lett. **30**, 3269-3271 (2005).
3. A. Kots and A. Paritsky, "Fiber optic microphone for harsh environment," Proc. SPIE **3852**, 106-112 (1999).
4. H. Bezzaoui and E. Voges, "Integrated optics combined with micromechanics on silicon," Sens. Actuators A **29**, 219-223 (1991).
5. N. Pelletier, B. Bêche, N. Tahani, J. Zyss, L. Camberlein, and E. Gaviot, "SU-8 waveguiding interferometric micro-sensor for gage pressure measurement," Sens. Actuators A **135**, 179-184 (2007).
6. M. Ohkawa, M. Izutsu, and T. Sueta, "Integrated optic pressure sensor on silicon substrate," Appl. Opt. **28**, 5153-5157 (1989).
7. G. N. De Brabander, J. T. Boyd, and G. Beheim, "Integrated optical ring resonator with micromechanical diaphragm for pressure sensing," IEEE Photon. Technol. Lett. **6**, 671-673 (1994).
8. G. N. De Brabander, G. Beheim, and J. T. Boyd, "Integrated optical micromachined pressure sensor with spectrally encoded output and temperature compensation," Appl. Opt. **37**, 3264-3267 (1998).
9. H. Porte, V. Gorel, S. Kiryenko, J. Goedgebuer, W. Daniau, and P. Blind, "Imbalanced Mach-Zehnder interferometer integrated in micromachined silicon substrate for pressure sensor," J. Lightwave Technol. **17**, 229-233 (1999).
10. M. Ohkawa, Y. Shirai, T. Goto, S. Sekine, and T. Sato, "Silicon-based integrated optic pressure sensor using intermodal Interference between TM-like and TE-like modes," Fiber and Integrated Optics **21**, 105-113 (2002).
11. H. Nikkuni, Y. Watanabe, M. Ohkawa, and T. Sato, "Sensitivity dependence with respect to diaphragm thickness in guided-wave optical pressure sensor based on elasto-optic effect," Opt. Eng. **47**, 044402 (2008).
12. M. Ohkawa, K. Hasebe, S. Sekine, and T. Sato, "Relationship between sensitivity and waveguide position on the diaphragm in integrated optic pressure sensors based on the elasto-optic effect," Appl. Opt. **41**, 5016-5021 (2002).
13. M. Tabib-Azar, and G. Beheim, "Modern trends in microstructures and integrated optics for communication, sensing, and actuation," Opt. Eng. **36**, 1307-1318 (1997).
14. P. Rai-Choudhury, *MEMS and MOEMS Technology and Applications* (SPIE Press, Washington, 2000).

#98914 - $15.00 USD Received 16 Jul 2008; revised 29 Aug 2008; accepted 1 Sep 2008; published 9 Sep 2008

1. Introduction

Lightwave sensing technology has attracted much interest due to its immunity to electromagnetic interference (EMI) and the impossibility of electric spark. Fiber optical sensors [1-3] have been energetically studied due to their inherent advantages, such as lightweight construction, simple configuration, and efficient interaction between the lightwave and the measurand. On the other hand, the guided-wave optical sensors [4-12] also have remarkable advantages, such as being alignment-free and having stout configuration. Moreover, as it is possible to integrate mechanical structures on a common substrate, these are favorable for mechanical sensors, including pressure sensors, accelerometers, and so on.

Pressure sensors are widely used in various fields such as industrial, medical, automotive and household fields. The excellent properties of the guided-wave optical pressure sensor are useful especially for medical applications which require EMI immunity, the impossibility of an electrical leak, etc., for safety and reliability reasons. One of expected applications of the sensor is blood pressure sensing, in which a pressure sensor incorporated into a catheter could be utilized [10]. Another application is acoustic sensing under strong electromagnetic fields such as in Magnetic Resonance Imaging (MRI) [3]. The pressure sensor could be utilized as a microphone for patient-to-physician communication during MRI operation. For both applications, the guided-wave optical pressure sensors are expected to operate normally, but the sensors must be designed to meet the required sensitivity and dynamic range.

Incidentally, the guided-wave optical sensor is generally classified into two types: amplitude-modulation-based [4] and phase-modulation-based [5-12]. Sensitivity of the phase-modulation-based sensor is, in many cases, higher than that of the amplitude-modulation-based sensor, although the phase-modulation-based sensor requires an intereferometric optical circuit. Phase-modulation-based guided-wave optical pressure sensors have already been demonstrated by several groups [5-12]. Our group has also developed silicon-based and glass-based guided-wave optical pressure sensors using intermodal interference between the fundamental TM-like and TE-like modes [10-12]. Our guided-wave optical pressure sensors have a diaphragm as a pressure-sensitive structure, and are based on the elasto-optic effect. Sensitivity of the sensors using the elasto-optic effect is theoretically known to be dependent on diaphragm dimensions, *i.e.* thickness, side length, and aspect ratio, in other words, the side length ratio of the rectangular diaphragm. In the design of the guided-wave optical pressure sensors, such dependencies must be examined experimentally.

In our previous study, the sensitivity was theoretically and experimentally found to be inversely proportional to the square of the diaphragm thickness [11]. However, sensitivity dependences with respect to side length and aspect ratio have yet to be experimentally studied. According to the theoretical results, the sensitivity is proportional to the cube of the side length. Moreover, a square diaphragm with an aspect ratio of 1 is appropriate to obtain higher sensitivity for two waveguide positions: the center and the edge of the diaphragm. In this study, sensitivity dependences on side length and aspect ratio were experimentally examined. The obtained experimental results agreed well with the theoretical predictions.

Incidentally, by the development of MEMS and MOEMS technologies, guided-wave optical sensors with micromachined structures have attracted intensive attention over the past few decades [13, 14]. Silicon is a familiar substrate in MEMS and MOEMS technologies, but glass was used as diaphragm material in this study. The use of glass is suitable in the comparison of theoretical and experimental results because the mechanical and optical parameters of glass are well known. The results obtained in this study can also provide valuable guidance in sensor design for silicon-based guided-wave optical pressure sensors.

2. Principles of operation

Figure 1 shows the configuration of the guided-wave optical pressure sensor using intermodal interference. A pressure sensor consisting of a rectangular diaphragm and a straight single-mode waveguide on the diaphragm is placed between a pair of crossed polarizers. The polarization of the input polarizer is set at 45° to each guided mode. When a pressure

#98914 - $15.00 USD Received 16 Jul 2008; revised 29 Aug 2008; accepted 1 Sep 2008; published 9 Sep 2008

difference between the upper and lower surfaces of the diaphragm is applied, the diaphragm deflects. The deflection causes strain in the diaphragm. By the elasto-optic effect, the strain induces change in the refractive index of the waveguide. The index change results in phase retardation of the guided light propagating in the waveguide. If the phase retardations of the two guided modes differ from each other, the phase difference is a function of the pressure difference. The output polarizer converts the polarization-modulated light into intensity-modulated light. The intensity sinusoidally changes with the pressure difference.

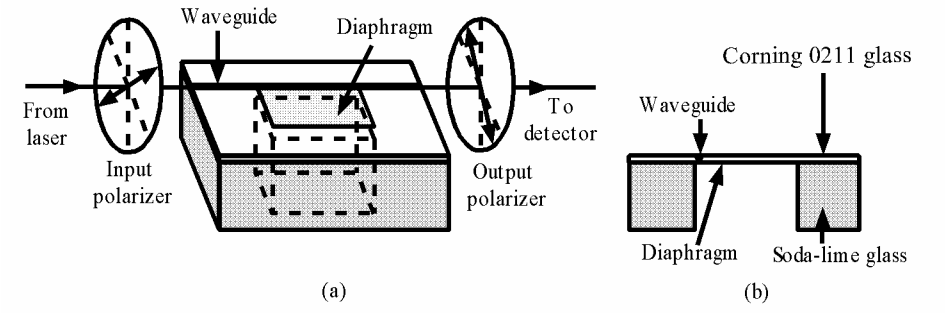

Fig. 1. (a) Configuration of the glass-based guided-wave optical pressure sensor placed between a pair of crossed polarizers and (b) its cross-section drawing.

3. Theory

3.1 Phase sensitivity versus side length of diaphragm

In this paper, phase sensitivity, defined as the phase difference per unit pressure, is utilized as the sensor sensitivity. The phase sensitivity was calculated as a function of the side length of the diaphragm, following the mathematical description [12]. In the calculation, it was assumed that pressure is uniformly applied to the square diaphragm with all edges clamped rigidly. The wavelength of guided light is set at 633 nm, and the diaphragm thickness at 0.22 mm. The theoretical calculations were carried out using the mechanical and optical parameters of Corning 0211 glass except for the photoelastic coefficients of fused silica. The coefficients of fused silica are similar to those of the glass, so the use of the photoelastic coefficients of fused silica does not result in a serious error to the theoretical results.

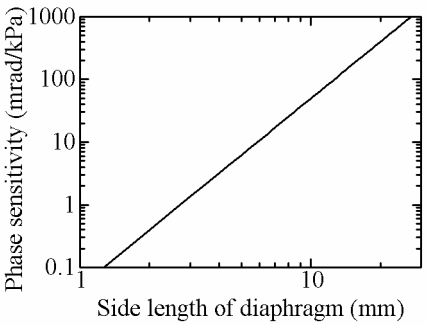

Fig. 2. Phase sensitivity as a function of the side length of the diaphragm for the waveguide on the center of the diaphragm.

Incidentally, the sensitivity is known to be dependent on the waveguide position on the diaphragm [12]. The phase sensitivity has the maximum value when the waveguide is placed across the diaphragm edge, but the sensitivity rapidly decreases when the waveguide deviates from the edge. On the other hand, when the waveguide is located at the center of the diaphragm, the sensitivity is not affected by a deviation of the waveguide position from the

#98914 - $15.00 USD Received 16 Jul 2008; revised 29 Aug 2008; accepted 1 Sep 2008; published 9 Sep 2008

center. Here, to avoid any undesirable influence due to the waveguide deviation, the center of the diaphragm was chosen as the waveguide position. Figure 2 shows the calculated phase sensitivity versus the side length of the diaphragm. The slope of the curve is 3 in the log-log graph of Fig. 2 since the phase sensitivity is proportional to the cube of the side length of the diaphragm.

3.2 Phase sensitivity versus aspect ratio of diaphragm

The phase sensitivity was calculated as a function of the aspect ratio of the diaphragm. In the calculation, the length of the side parallel to the waveguide, that is, the interaction length, was set to be 10 mm. Also, the center and edge of the diaphragm were chosen as waveguide positions. All other assumptions were the same as in Section 3.1. Figures 3(a) and 3(b) indicate the calculated results for the waveguides across the center and the edge of the diaphragm, respectively. As shown in Fig. 3(a), the sensitivity of the waveguide along the center peaks when the aspect ratio of the diaphragm is approximately 1. On the other hand, the sensitivity of the waveguide along the edge increases along with the aspect ratio when the aspect ratio is less than 1, whereas the sensitivity reaches a plateau when the ratio is more than 1, as shown in Fig. 3(b).

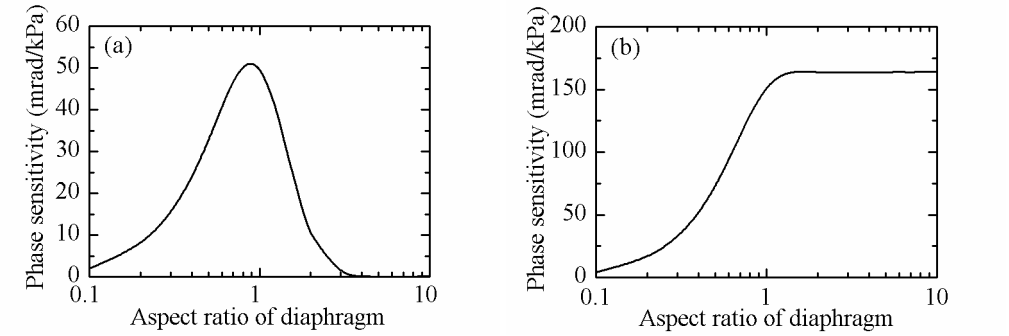

Fig. 3. Phase sensitivity as a function of aspect ratio of the diaphragm for the waveguides along (a) the center and (b) the edge of the diaphragm.

4. Experiments

4.1 Fabrication

The guided-wave optical pressure sensors were built using two glass substrates: a Corning 0211 glass as a diaphragm plate and a soda-lime glass with a rectangular hole as a support structure of the diaphragm. First, a thin layer of aluminum was evaporated on the Corning glass. Photoresist was deposited by a spin-coating method on the glass. Next, the waveguide pattern was engraved on the aluminum film by a photolithographic process. Then, the glass was immersed in KNO_3 for two hours at 400 °C to form the single-mode channel waveguides spaced 0.5 mm apart. After waveguide formation, the waveguides were adjusted to be parallel to the diaphragm edge, and then the two substrates were bonded together by UV adhesion.

Table 1 shows the dimensions of the fabricated guided-wave optical pressure sensors for sensitivity dependences on side length and aspect ratio of the diaphragm. In order to determine the relationship between the sensitivity and the side length of the diaphragm, four sensors with diaphragms of 7 mm×7 mm×0.22 mm (Sensor #1), 10 mm×10 mm×0.22 mm (Sensor #2), 14 mm×14 mm×0.22 mm (Sensor #3), and 20 mm×20 mm×0.22 mm (Sensor #4) were fabricated. Moreover, three sensors with diaphragms of 5 mm×10 mm×0.22 mm (Sensor #5), 15 mm×10 mm×0.22 mm (Sensor #6), and 20 mm×10 mm×0.22 mm (Sensor #7) were fabricated in addition to Sensor #2 in order to examine the sensitivity dependence on the aspect ratio of the diaphragm.

#98914 - $15.00 USD Received 16 Jul 2008; revised 29 Aug 2008; accepted 1 Sep 2008; published 9 Sep 2008

Table 1. Dimensions of the fabricated guided-wave optical pressure sensors for sensitivity dependences on side length and aspect ratio of the diaphragm.

	Sensor	Side length perpendicular to waveguide (mm)	Side length parallel to waveguide (mm)	Thickness (mm)
Sensitivity dependence on side length of the diaphragm	#1	7	7	0.22
	#2	10	10	0.22
	#3	14	14	0.22
	#4	20	20	0.22
Sensitivity dependence on aspect ratio of the diaphragm	#5	5	10	0.22
	#2	10	10	0.22
	#6	15	10	0.22
	#7	20	10	0.22

4.2 Experimental setup

Output intensity versus applied pressure was measured to evaluate the phase sensitivity of the fabricated sensors. Figure 4 illustrates the experimental setup. A linearly-polarized He-Ne laser at 633 nm was employed as the light source. The polarization of the laser beam was adjusted to be 45° to the sensor surface, and thus an input polarizer as shown in Fig. 1 was not needed. A syringe was connected to the sensor with a silicone tube, and pressure was applied to the diaphragm by pulling and pushing the plunger of the syringe. The applied pressure was determined from the ideal gas law. A positive pressure value means that the applied pressure is higher than the atmospheric pressure. A pinhole was utilized to block any stray light, and the output intensity through the pinhole was measured by the photodetector.

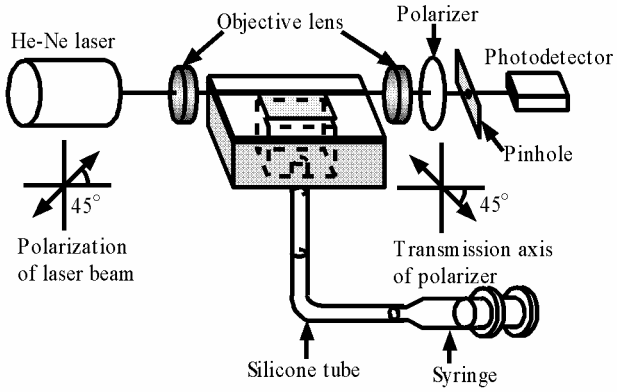

Fig. 4. Experimental setup for measuring the output intensity versus the pressure in the guided-wave optical pressure sensor.

4.3 Experimental results and discussions

4.3.1 Phase sensitivity versus side length of diaphragm

Figures 5(a)-(d) show the output intensity versus the applied pressure for the waveguide nearest to the center of the diaphragm in Sensors #1-4, respectively. Dots in each figure indicate the measured values, and solid line shows the computer projection of the

#98914 - $15.00 USD Received 16 Jul 2008; revised 29 Aug 2008; accepted 1 Sep 2008; published 9 Sep 2008

experimental data. The output intensity sinusoidally changes with the applied pressure. A half period of the output intensity is called the halfwave pressure. The halfwave pressure corresponds to π rad of the phase difference. From Figs. 5(a)-(d), the halfwave pressures of Sensors #1-4 were evaluated to be 201 kPa, 61 kPa, 29 kPa, and 10 kPa, corresponding to the phase sensitivities of 16 mrad/kPa, 52 mrad/kPa, 108 mrad/kPa, and 314 mrad/kPa, respectively.

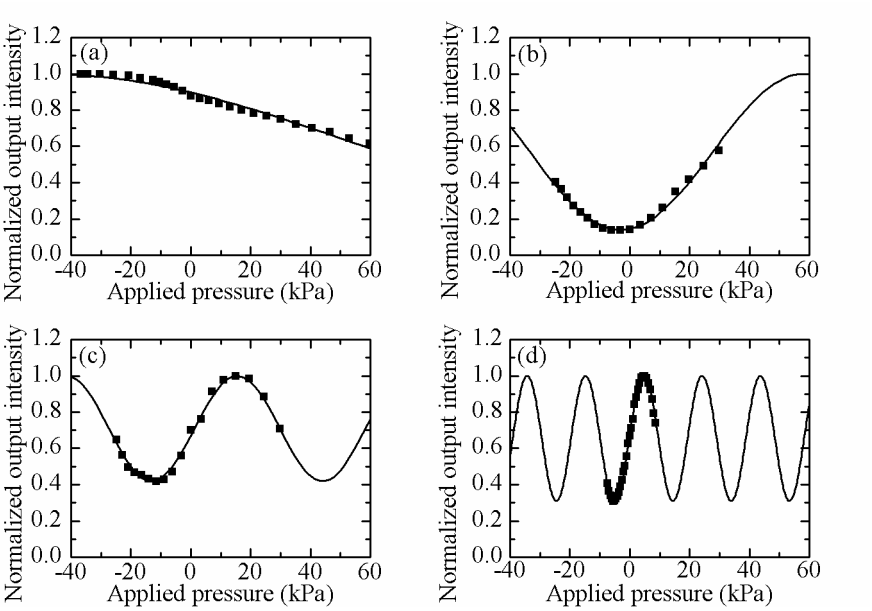

Fig. 5. Normalized output intensity versus applied pressure for the waveguide nearest to the center of the diaphragm. Figures (a)-(d) are for Sensors #1-4, respectively.

Table 2 and Fig. 6 show the calculated and measured sensitivities of Sensors #1-4. The measured sensitivities of Sensors #1 and #2 almost agree with the theoretical estimations, while the measured values of Sensors #3 and #4 were about 80 % of the theoretical ones. The cause of such slight difference has yet to be identified. However, the measured sensitivity was found to be almost proportional to the cube of the side length of the diaphragm.

Table 2. Calculated and measured sensitivities of Sensors #1-4.

Sensor	Diaphragm dimensions (mm×mm×mm)	Calculated sensitivity (mrad/kPa)	Measured sensitivity (mrad/kPa)
#1	$7 \times 7 \times 0.22$	17	16
#2	$10 \times 10 \times 0.22$	50	52
#3	$14 \times 14 \times 0.22$	137	108
#4	$20 \times 20 \times 0.22$	399	314

#98914 - $15.00 USD Received 16 Jul 2008; revised 29 Aug 2008; accepted 1 Sep 2008; published 9 Sep 2008

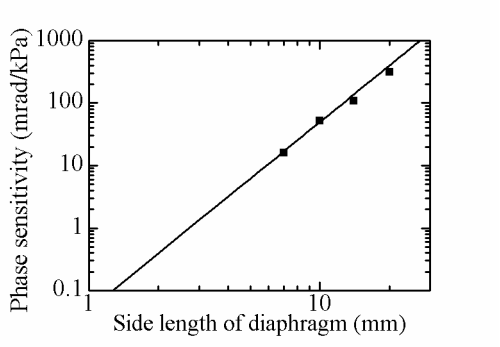

Fig. 6. Sensitivity dependence on the side length of the diaphragm for the waveguide nearest to the center of the diaphragm. Dots show the measured sensitivities of Sensors #1-4. Solid line shows the calculated sensitivity as a function of the side length.

4.3.2 Phase sensitivity versus aspect ratio of diaphragm

Figures 7(a)-(c) show the output intensity versus the applied pressure for the waveguide nearest to the center of the diaphragm in Sensors #5-7, respectively. From Figs. 7(a)-(c), the halfwave pressures of Sensors #5-7 were evaluated to be 102 kPa, 130 kPa, and 313 kPa, corresponding to the phase sensitivities of 31 mrad/kPa, 24 mrad/kPa, and 10 mrad/kPa, respectively. Figures 8(a)-(d) indicate the output intensity versus the applied pressure for the waveguide nearest to the edge of the diaphragm of Sensors #5, #2, #6, and #7, respectively. From Figs. 8(a)-(d), the halfwave pressures of Sensors #5, #2, #6, and #7 were measured to be 75 kPa, 34 kPa, 30 kPa, and 24 kPa, corresponding to the phase sensitivities of 42 mrad/kPa, 92 mrad/kPa, 105 mrad/kPa, and 131mrad/kPa, respectively.

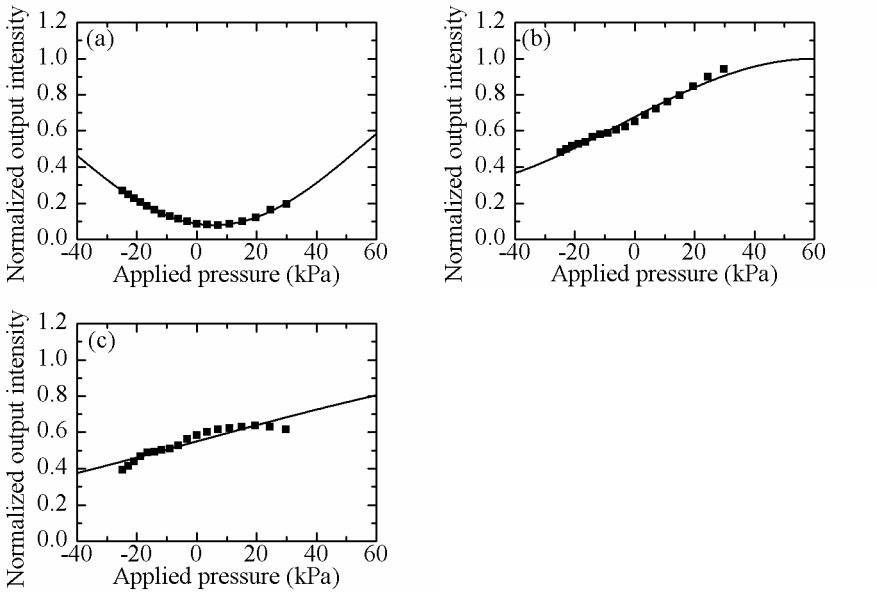

Fig. 7. Normalized output intensity versus applied pressure for the waveguide nearest to the center of the diaphragm. Figures (a)-(c) are for Sensors #5-7, respectively.

#98914 - $15.00 USD Received 16 Jul 2008; revised 29 Aug 2008; accepted 1 Sep 2008; published 9 Sep 2008

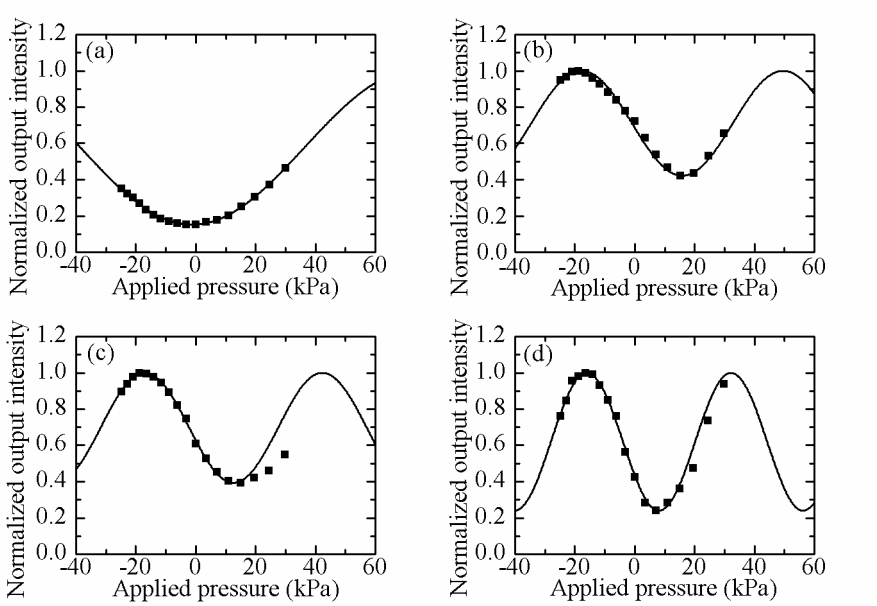

Fig. 8. Normalized output intensity versus applied pressure for the waveguide nearest to the edge of the diaphragm. Figures (a)-(d) are for Sensors #5, #2, #6, and #7, respectively.

Table 3 and Fig. 9 show the calculated and measured sensitivities of Sensors #2 and #5-7. Figures 9(a) and (b) are for the waveguides nearest to the center and nearest to the edge, respectively. For the waveguide located nearest to the center, the measured sensitivities almost match the theoretical ones, as shown in Table 3 and Fig. 9(a). Moreover, the highest sensitivity was determined to be when the aspect ratio is around 1. For the waveguide nearest to the edge, the measured sensitivities were considerably different from the theoretical ones, as shown in Table 3 and Fig. 9(b). The difference was partially caused by deviation from the diaphragm edge of the waveguide. The deviations for Sensors #5, #2, #6, and #7 were 0.30 mm, 0.36 mm, 0.39 mm, and 0.05 mm, respectively. The theoretical sensitivities were recalculated to be 46 mrad/kPa, 108 mrad/kPa, 117 mrad/kPa, and 157 mrad/kPa, taking into account of the waveguide deviations. The measured sensitivities are about 80 % of the recalculated ones based on the actual waveguide position. A slight difference still remains, but the measured results show the same tendency as the theoretical estimations. The experimental results qualitatively support the theoretical ones described in Section 3.2. The measured sensitivities which are lower than the theoretical ones are attributed to relaxation of the induced strain near the diaphragm edge. Such relaxation was mainly caused by imperfect bonding by UV adhesion, which reduced the rigidity of the structure surrounding the diaphragm.

#98914 - $15.00 USD Received 16 Jul 2008; revised 29 Aug 2008; accepted 1 Sep 2008; published 9 Sep 2008

Table 3. Calculated and measured sensitivities of Sensors #2 and #5-7.

Sensor	Diaphragm dimensions (mm×mm×mm)	The center of the diaphragm		The edge of the diaphragm	
		Calculated sensitivity (mrad/kPa)	Measured sensitivity (mrad/kPa)	Calculated sensitivity (mrad/kPa)	Measured sensitivity (mrad/kPa)
#5	$5 \times 10 \times 0.22$	33	31	72	42
#2	$10 \times 10 \times 0.22$	50	52	151	92
#6	$15 \times 10 \times 0.22$	28	24	164	105
#7	$20 \times 10 \times 0.22$	10	10	164	131

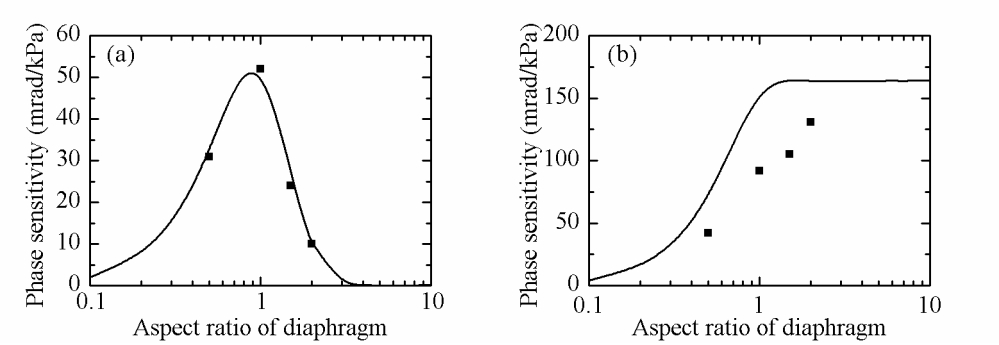

Fig. 9. Sensitivity dependence on the aspect ratio of the diaphragm for two waveguide positions: (a) nearest to the center and (b) nearest to the edge. Dots show the measured sensitivities of Sensors #2 and #5-7. Solid lines show the calculated sensitivities as a function of the aspect ratio.

5. Conclusions

Sensitivity dependences on side length and aspect ratio of the diaphragm in a glass-based guided-wave optical pressure sensor were experimentally examined in this study. The sensitivity was almost proportional to the cube of the side length. Regarding dependence on the aspect ratio of the diaphragm, the measured sensitivities peaked when the aspect ratio was around 1, the same as the theoretical prediction, for the waveguide nearest to the center of the diaphragm. Moreover, for the waveguide nearest to the edge of the diaphragm, the measured sensitivities showed the same tendency as the theoretical estimations, that is, sensitivity reaches a plateau when the aspect ratio is greater than 1.

Acknowledgments

This work was, in part, supported by a Grant-in-Aid for Scientific Research (17360157) from the Japan Society for the Promotion of Science.

#98914 - $15.00 USD Received 16 Jul 2008; revised 29 Aug 2008; accepted 1 Sep 2008; published 9 Sep 2008